*33rd EPS Conference on Plasma Phys. Rome, 19 - 23 June 2006 ECA Vol.**30I**, O-3.013 (2006)*

Experimental study of plasma-surface interaction under heat loads expected for ITER transient events

V.I. Tereshin[1], I.E. Garkusha[1], V.V. Chebotarev[1], I.S. Landman[2], M.S. Ladygina[1], V.A. Makhlaj[1], D.G. Solyakov[1], A.V. Tsarenko[1]

[1] *Institute of Plasma Physics of the NSC KIPT, Kharkov, 61108, Ukraine*
[2] *Forschungszentrum Karlsruhe, IHM, 76021 Karlsruhe, Germany*

Introduction

Plasma-surface interaction (PSI) during the transient events in ITER is among the most important issues determining the tokamak performance and the lifetime of plasma-facing components. ITER transient loads will result in both material erosion and plasma contamination by impurities. For disruptions, the heat loads to ITER divertor components are anticipated to be of an order Q_{disr}= (10-100) MJ/m^2 (load duration t = (1–10) ms) [1,2]. ITER ELMs may also lead to unacceptable lifetime [3,4]; their loads are estimated as Q_{ELM}= (1-3) MJ/m^2 at t = (0.1–1) ms and the repetition frequency of an order of 1 Hz [1].

Because the energy range of ITER disruptions and ELMs is far above of that in available tokamaks, numerical codes [5,6] and experimental simulation with other powerful plasma devices [7,8] are engaged for analysis of PSI features in tokamak-reactor such as vapor shielding and its influence on plasma energy transfer to the surface, erosion mechanisms of plasma facing materials, impurities transport in the plasma. The quasi-steady-state plasma accelerators (QSPA) provide the most adequate simulation of ITER transient events.

Strong shielding effect under the plasma energy transfer to the material surface in disruption simulation experiments was studied mainly for graphite targets [7,8]. For the ELMs, and their impact to the tungsten surface, the shielding layer properties were not investigated yet. This paper presents the results of quasi-steady-state plasma streams interaction with material surfaces under conditions typical for ITER disruptions and type I ELMs, including analysis of plasma energy transfer to the material surface in dependence on impacting load, vapor shield dynamics for different materials and erosion of tungsten.

1. Experimental Setup and Diagnostics

Experiments were carried out in the quasi-steady-state plasma accelerator QSPA Kh-50 described elsewhere [9]. It consists of two stages. The first one is used for plasma production. The second stage is a coaxial system of shaped active electrodes with magnetically screened elements. Plasma streams were injected into magnetic system of 1.6 m in length and 0.44 m in inner diameter with magnetic field up to 0.72 T [10]. Targets of different materials were exposed to plasma with various numbers of pulses (duration - 250 μs, ion energy ≤ 0.6 keV, heat load: (0.5-2.5) MJ/m^2, typical for ELM, or up to 25 MJ/m^2, typical for ITER disruptions).

The main plasma diagnostics were as follows: spectroscopy, laser interferometry, high-speed imaging, local calorimeters, pyroelectric bolometers, etc. The surface roughness was measured by Hommelwerke tester T500. Surface analysis was carried out with an optical microscope MMR-4, equipped with CCD camera. Weight losses were measured also.

2. Results of Experiments

2.1. Disruption simulation.

2.1.1. Vapor shield effects. The key feature of plasma-surface interaction under disruption heat loads is vapor shield formation in front of the exposed surface. Temporal and spatial

distributions of plasma density in the shielding layer were obtained with laser interferometry. The plasma density in the shield is more than one order of magnitude higher in comparison with that in impacting plasma. The thickness of the shielding layer, formed close to the graphite target, being equal (1-2) cm for sample irradiation with no magnetic field, exceeds 5 cm for B_{z0} = 0.72 T (Fig. 1). Formation of dense plasma layer in front of the surface protects the material from the contact with impacting plasma. Shielding efficiency of carbon vapor is analyzed in [7,8], and, typically, only few percents of impacting plasma energy reached the surface for disruption plasma loads. Dissipation of the plasma stream energy in the shielding layer results in shield expansion, heating and re-irradiation by the shield.

To study the influence of target atomic mass on the shield dynamics, tungsten, copper, titanium, aluminum, fluoroplastic F_4C and graphite targets were used. Spatial distributions of evaporated materials at the vicinity of the target were obtained using corresponding intensities of ion spectral lines (Fig.2). As it follows from this figure, the evaporated material with higher atomic weight is more "pressed" to the target due to the lower thermal velocities and diffusion coefficient. Despite of an intense W-surface melting it was impossible to draw its distribution in the shield, as far as its thickness is comparable with spatial resolution of applied diagnostic.

Measurements of plasma radiation (with $\lambda \leq 3000$ Å) were performed with pyroelectric bolometer. One can see from Fig.3 that intensity of radiation from the shield is by (7-10) times higher in comparison with free plasma stream. Maximum of radiation is registered from thin region (~ 5 mm) corresponding to periphery zone of the shield (2-3 cm from the surface).

2.1.2. Surface erosion. The disruption simulation experiments showed that the melt motion driven by plasma pressure gradient dominates in tungsten macroscopic erosion, resulting in droplet splashing and formation of the craters with rather large edge ridges of displaced material. The height of the ridge achieves (130-240) μm for 75 pulses. The high value of the surface roughness masks the erosion crater. The melt motion is accompanied by splashing of the metal droplets with the sizes up to 100 μm onto unexposed target surface. Influence of plasma pressure gradient on macroscopic erosion of tungsten and other metals for perpendicular and inclined exposures is described in details in [11, 12].

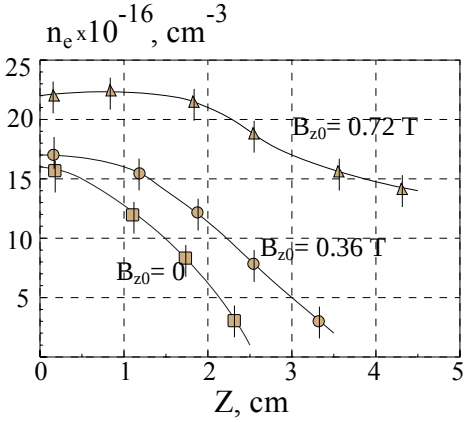

Fig. 1. Plasma shield density vs. the distance from the target surface (25 MJ/m^2, $\Delta\tau$ = 20 μs from the beginning of plasma interaction with the surface).

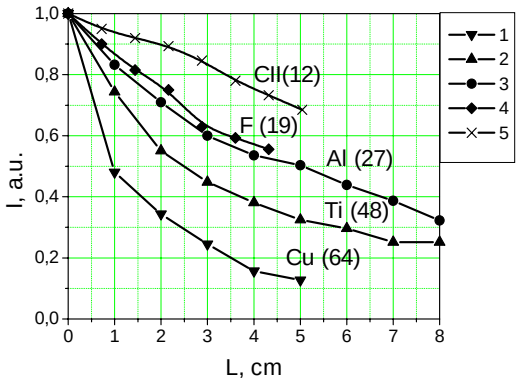

Fig.2. Spatial distributions of evaporated materials in front of the surface for different exposed targets evaluated from spectral lines: CuII (2590Å), TiII (4534Å), AlII (5593Å), FII (4109Å) and CII (4267Å).

2.2. ELM simulation experiments

2.2.1. Onsets of tungsten melting and evaporation under ELM-like plasma loads. These experiments were aimed to investigate the plasma energy transfer to the material

surface in dependence on impacting load under repetitive plasma exposures with ELM. Fig. 4 shows the heat load to the tungsten surface, measured with calorimeter for different energy of impacting plasma stream. Onset of tungsten melting is observed on the target surface at heat load of 0.57 MJ/m^2. The measurements shows that even for plasma exposures, which not result in the melting, the target heat load is about (55-60) % of the impact plasma energy. Vapor shield formation and its influence on plasma energy transfer to the surface is seen for surface load achieving 1.1 MJ/m^2. The fraction of plasma energy, transferred to the surface, is rapidly decreased with achieving the evaporation onset for targets. At this, the value of heat load to the surface is practically constant with further increase of the incident plasma energy.

Dynamics of tungsten vapor in front of the target surface has been studied with high-speed photography. It was shown that evaporated tungsten concentrated in rather thin plasma layer of < 0.5 cm close to the surface. This could be explained by large atomic mass of tungsten and impacting plasma pressure. In the case of graphite target exposure the thickness of the shield was increased during the pulse and achieved 5 cm.

2.2.2. Tungsten erosion under the repetitive ELM-like plasma loads. Erosion of the tungsten surface in the course of large number of repetitive pulses was studied for plasma exposures with surface heat loads of 0.45 MJ/m^2 (below the melting threshold), 0.75 MJ/m^2 (resulting in melting) and 1.1 MJ/m^2 (evaporation). It was found that surface damage under the plasma exposures below the melting threshold is mainly caused by macroscopic cracks. First plasma pulses form main network of the cracks with the cell size of ~ 1 mm (Fig. 5). The crack network is stable, after a large number of exposures the enlargement of the cracks and their penetration in the depth is observed. Small material pieces (of (12-20) μm in size) may appear inside the crack meshes due to bifurcations of large cracks. The subsequent separation of such pieces from the bulk does not result in their ejection, but it immediately leads to the piece melting because of decreased heat conduction (Fig.5). The erosion rate obtained from mass loss measurements is 1.2 nm/pulse. This can be explained by contribution of sputtering.

Tungsten exposures with surface heat loads increased up to 0.75 MJ/m^2 resulted in appearing the melt layer with the thickness of tens μm. The melting process leads to considerably increased surface roughness. Besides the large-size cracks, fine intergranular cracks with network of (10-30) μm were additionally found on resolidified surface. Fine cracks trigger qualitative evolution of the sample surface starting after two hundreds of pulses, which is accompanied by growing mass loss rate.

With increasing surface heat load up to 1.1 MJ/m^2, the boiling bubbles are observed on the target surface. The boiling is initiated at the surface by impurities. With increasing the number of exposures it becomes predominantly volumetric and deep bubbles are arisen at the surface. The volumetric boiling occurs mainly at the vicinity of large crack edges. The boiling results

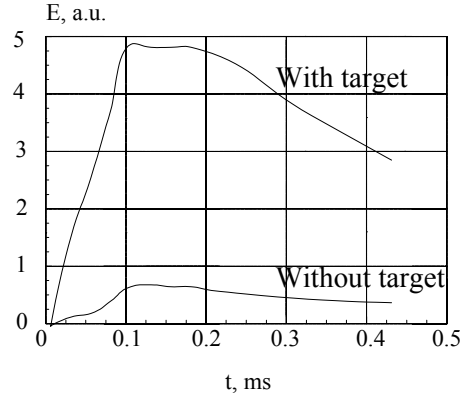

Fig. 3. Intensity of the shielding layer radiation measured with $LiNbO_3$ detector.

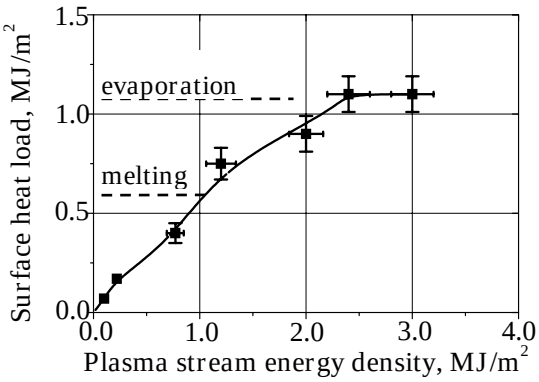

Fig. 4. Heat load to the tungsten surface vs. energy density of impacting plasma stream.

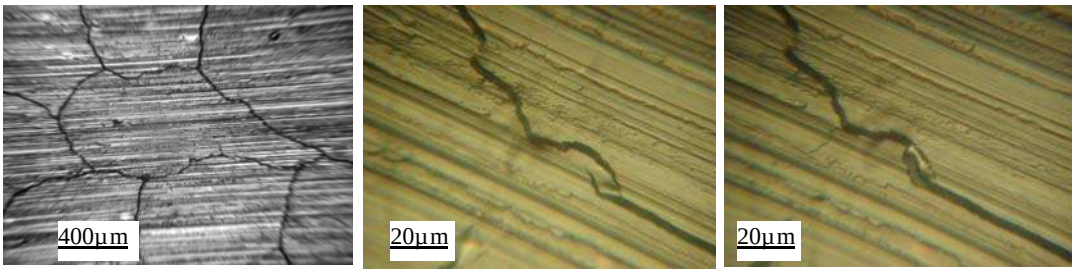

Fig.5. Mesh of cracks at the tungsten surface, crack bifurcation, and melting of the separated piece.

in intensification of the droplets splashing. The drop size is varied in the range of (5-100) µm. The corrugations and pits are appeared at the surface after 200 pulses, like for exposure with 0.75 MJ/m^2. So, this threshold number doesn't depend on impact and target heat loads. It is possibly determined by thermo-physical tungsten properties. The mass loss rate in this regime is (0.036-0.04) mg/cm^2 per pulse. This value is by 10 times higher than for exposures with surface load of 0.75 MJ/m^2. Thus, the boiling essentially adds to the mass losses.

Conclusions

Plasma exposures of materials were performed with repetitive pulses of the time duration of 250 µs, ion energy ≤ 0.6 keV, and the heat load varied in the range of (0.5-25) MJ/m^2.

Analysis of influence of target atomic mass on the shield dynamics showed that the evaporated material of the target with higher atomic weight became more pressed to the target surface and thickness of the shield was decreased. In particular, evaporated tungsten is concentrated in rather thin plasma layer of < 0.5 cm close to the surface.

The fraction of plasma energy, absorbed by the target, is in dependence on impacting load and is rapidly decreased with achieving the evaporation onset for exposed targets.

Erosion of tungsten surface was studied in the course of large number of repetitive pulses with different values of the surface heat loads. The surface damage under the plasma exposures below the melting threshold is mainly caused by macroscopic cracks. The melting process leads to increased surface roughness. Besides the large-size cracks, fine intergranular cracks with network of (10-30) µm are also found on resolidified surface. The evaporation results in enhanced mass losses of tungsten: increase of the heat load from 0.75 to 1.1 MJ/m^2 raises mass losses by one order of magnitude and causes bubble structures at the surface.

References

1. G. Federici et al., *Plasma Phys. Control. Fusion* 45, (2003)1523.
2. A. Loarte et al., *Plasma Phys. Control. Fusion* 45, (2003)1549.
3. T. Eich et al., *J. Nucl. Mater.* 337-339, (2005) 669-676.
4. G. Janeschitz et al., *J. Nucl. Mater.* 290-293, (2001) 1.
5. I. Landman et al., *J. Nucl. Mater.* 337-339, (2005)761-765.
6. A. Hassanein, I. Konkashbaev, *J. Nucl. Mater.*313-316, (2003) 664.
7. V.V. Chebotarev et al., *J. Nucl. Mater.* 233-237 (1996) 736.
8. N. I. Arkhipov et al., *Fus. Eng. and Design* 49-50, (2000)151.
9. A. I. Morozov et al., *Plasma Devices and Operations* 2, (1992)155-165.
10. V. I.Tereshin et al., *Brazilian Journal of Physics* 32, № 1, (2002)165-171.
11. V. I. Tereshin et al., *J. Nucl. Mater.* 313-316, (2003) 685-689.
12. I. E. Garkusha et al., *J. Nucl. Mater.* 337-339, (2005) 707-711.